Discovery of potent inhibitors of the *lyso*phospholipase autotaxin

Pritom Shah, Anne Cheasty, Caroline Foxton, Tony Raynham, Muddasar Farooq, Irene Farre Gutierrez, Aurore Lejeune, Michelle Pritchard, Andrew Turnbull, Leon Pang, Paul Owen, Susan Boyd, Alexandra Stowell, Allan Jordan, Niall M. Hamilton, James R. Hitchin, Martin Stockley, Ellen MacDonald, Mar Jimenez Quesada, Elisabeth Trivier, Jana Skeete, Huib Ovaa, Wouter H. Moolenaar, Hamish Ryder

PII: S0960-894X(16)31064-2
DOI: http://dx.doi.org/10.1016/j.bmcl.2016.10.036
Reference: BMCL 24339

To appear in: *Bioorganic & Medicinal Chemistry Letters*

Received Date: 31 August 2016
Revised Date: 11 October 2016
Accepted Date: 12 October 2016

Please cite this article as: Shah, P., Cheasty, A., Foxton, C., Raynham, T., Farooq, M., Gutierrez, I.F., Lejeune, A., Pritchard, M., Turnbull, A., Pang, L., Owen, P., Boyd, S., Stowell, A., Jordan, A., Hamilton, N.M., Hitchin, J.R., Stockley, M., MacDonald, E., Quesada, M.J., Trivier, E., Skeete, J., Ovaa, H., Moolenaar, W.H., Ryder, H., Discovery of potent inhibitors of the *lyso*phospholipase autotaxin, *Bioorganic & Medicinal Chemistry Letters* (2016), doi: http://dx.doi.org/10.1016/j.bmcl.2016.10.036

Discovery of potent inhibitors of the *lyso*phospholipase autotaxin

Pritom Shah[a,*], Anne Cheasty[a], Caroline Foxton[a], Tony Raynham[a], Muddasar Farooq[a], Irene Farre Gutierrez[a], Aurore Lejeune[a], Michelle Pritchard[a], Andrew Turnbull[a], Leon Pang[a], Paul Owen[a], Susan Boyd[a], Alexandra Stowell[c], Allan Jordan[c], Niall M. Hamilton[c], James R. Hitchin[c], Martin Stockley[a], Ellen MacDonald[a], Mar Jimenez Quesada[a], Elisabeth Trivier[a], Jana Skeete[a], Huib Ovaa[b,d], Wouter H. Moolenaar[b] and Hamish Ryder[a]

[a]*Cancer Research Technology, Discovery Laboratories, Babraham Research Campus, Cambridge, CB22 3AT, UK*
[b]*Netherlands Cancer Institute, Plesmanlaan 121, 1066 CX, Amsterdam, The Netherlands*
[c]*Drug Discovery Unit, Cancer Research UK Manchester Institute, The University of Manchester, Wilmslow Road, Manchester, M20 4BX, UK*
[d]*Current address: Department of Chemical Immunology, Leiden University Medical Center, Einthovenweg 20, 2333 ZC, Leiden, The Netherlands*

Keywords:
Autotaxin (ATX)
*Lyso*phosphatidic acid (LPA)
*Lyso*phosphatidylcholine (LPC)
Cancer

Autotaxin (ATX), also known as ectonucleotide pyrophosphatase/phosphodiesterase family member 2 (ENPP2), is a secreted lysophospholipase D (lysoPLD) that cleaves choline from lysophosphatidylcholine (LPC) forming lysophosphatidic acid (LPA), a mitogen and motility factor that has been implicated in the pathophysiology of cancer[1-3] and many other biological processes such as vascular development, lymphocyte homing and inflammation.[4-6] LPA consists of a single fatty acyl chain, a glycerol backbone and a free phosphate group. Several structurally diverse forms of LPA exist with different acyl-chain lengths and saturations. LPA acts through a number of LPA receptors and the great variety of cellular and biological actions of LPA is explained by the fact that the six known LPA receptors show broad tissue expression and can couple to at least three distinct G proteins, which, in turn, feed into multiple effector systems.[7] (Figure 1).

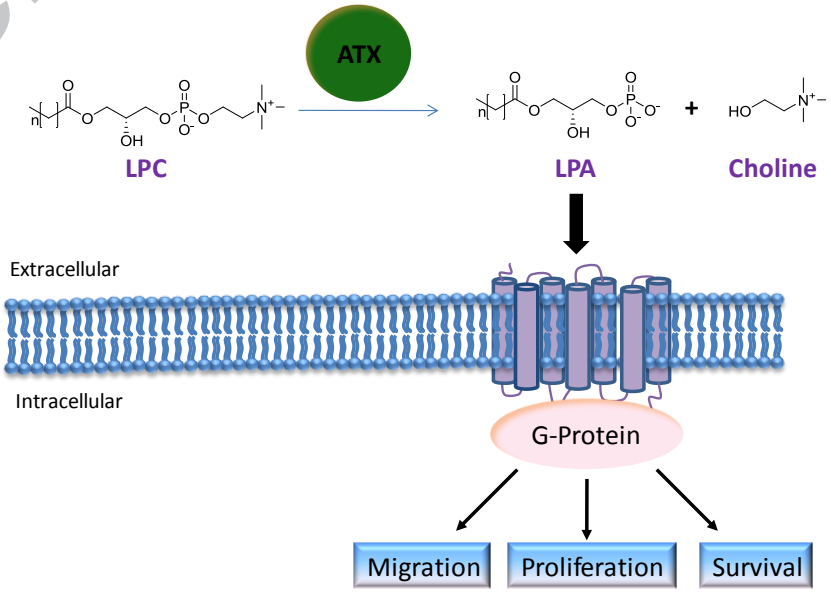

Figure 1. The Autotaxin-LPA axis showing conversion of LPC to LPA mediated by autotaxin and subsequent activation of LPA receptors

The ATX-LPA axis has been implicated in several disease states including inflammation,[8] pulmonary fibrosis,[9] and tumour progression.[10] ATX is processed along the classical export pathway and secreted as a catalytically active glycoprotein. ATX's major lipid substrate, LPC, is secreted by the liver and is abundantly present in plasma and interstitial fluids. Potent and selective inhibitors of ATX would clearly be of value to elucidate the biology of this target and an overview of the patent and primary literature describing the development of novel ATX inhibitors has recently been published.[11] Clinical trials have recently been initiated with GLPG1690 which is the first autotaxin inhibitor to enter the clinic and is under evaluation for the treatment of idiopathic pulmonary fibrosis.[12] Herein we report the discovery of a new class of small molecule inhibitors of ATX which have been optimized to deliver compounds suitable for *in vivo* studies.

A high throughput biochemical screen using the FS-3 assay[13] was run using the CRT compound collection of 87,865 compounds. The screen was run at 30 μM and the confirmed hit rate, defined as giving >50% inhibition at 30 μM, was 1.2%. After IC_{50} determination in the FS-3 assay, a number of distinct chemical series were identified. Compounds from each series were then screened in the enzyme coupled (EC) biochemical assay which uses the more physiologically relevant substrate LPC C16:0 and measures the release of choline.[14] The absolute potencies of the compounds in the enzyme coupled biochemical assay were generally lower and this helped prioritise between the chemical series so that chemistry effort could be focused on the most promising scaffolds. Based on the potency, ligand effiency (LE) and chemical tractability, the imidazo[4,5-*b*]pyridine **1** (Table 1) was selected as an attractive starting point for further chemistry.

Table 1. Profile of hit compound 1 selected for further optimisation

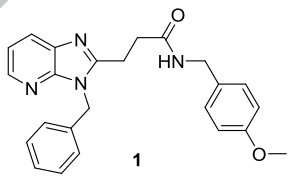

1

FS-3 IC_{50} (μM)[a]	EC IC_{50} (μM)[b]	LE[c]	cLogP[d]	PSA[e]	MWt
0.040	0.473	0.29	3.1	69	400

[a]The FS-3 biochemical assay utilizes a doubly labelled analogue of LPC wherein the fluorophore is quenched through intramolecular energy transfer. Hydrolysis of the substrate produces an increase in fluorescence. [b]EC IC_{50} - this assay utilises LPC C16:0 as substrate and measures the release of choline. [c]LE = Ligand Effiency = (1.36*pIC_{50})/HAC, HAC = heavy atom count, [d]cLogP is the ocatanol/water partition coefficient calculated using Stardrop™, [e]PSA = Polar Surface Area calculated using Stardrop™.

Compounds, prepared to explore the structure activity relationships of the hit **1**, were synthesized by the routes described in Schemes 1-4. The route used to modify the amide group (R^2 in compound **9**) and the N-benzyl group on the core (R^1 in compound **9**) is shown in Scheme 1. Thus, 2-chloro-3-nitro-pyridine was reacted with Cs_2CO_3 and the appropriate amine **3** in methanol at reflux to give **4** *via* a S_NAr reaction. The nitro group in **4** was hydrogenated over 10% Pd/C in ethanol to afford pyridine-2,3-diamine **5**. This diamine could alternatively be obtained through a reduction of the nitro group with iron in HCl. Compound **5** was reacted with succinic anhydride in dioxane at reflux and then treated with sulphuric acid in ethanol under reflux to give the ester **6**. Reaction of **6** with KO^{t}Bu and

the appropriate amine **8** in the microwave at 150°C afforded the final compounds of general formula **9**. Alternatively the carboxylic acid **7** obtained from the reaction of **5** with succinic anhydride, was treated with HBTU, triethylamine and the required amine **8** at room temperature to afford **9**. Alternative coupling agents can also be used to perform this amide formation.

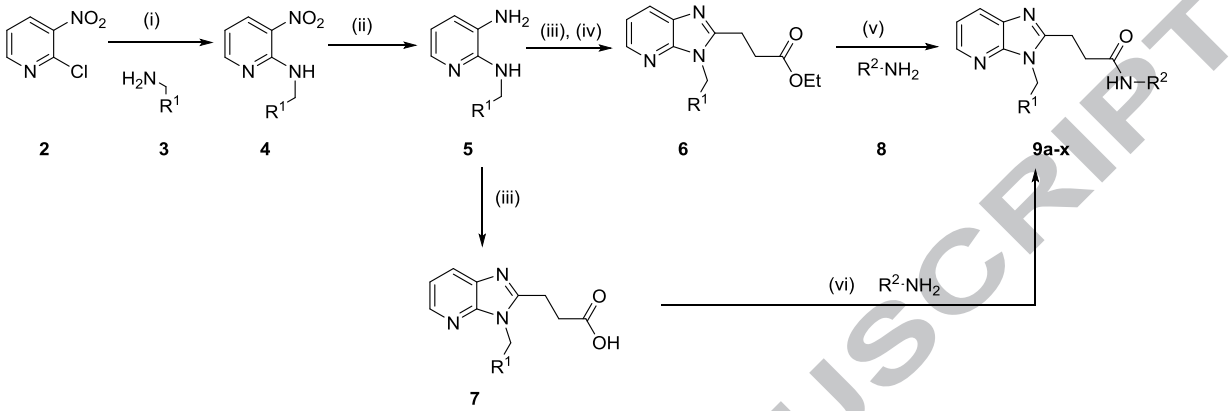

Scheme 1. Synthesis of imidazo[4,5-b]pyridine derivatives **9**. Reagents and conditions: (i) Cs_2CO_3, $R^1CH_2NH_2$, MeOH reflux, 61-100%; (ii) H_2, 10% Pd/C, EtOH, 1atm or cHCl, Fe powder, EtOH, 88-100%; (iii) succinic anhydride, dioxane, reflux, 52-81%; (iv) cH_2SO_4, EtOH, 10-13% combined yield for steps (iii) and (iv); (v) KO^tBu, R^2NH_2, MW, 4-42%; (vi) HBTU, Et_3N, R^2NH_2, 35-79%

The synthesis of compounds in which the ethyl linker has been modified to the carbamate and urea derivatives **13, 14** and **15** is shown in Scheme 2. Thus the diamine **5** was reacted with glycolic acid to give the alcohol **10** followed by Mitsunobu reaction with phthalimide to give **11**. Deprotection with hydrazine gave the amine **12** which was derivatised to the carbamate **13** and ureas **15a-b**. The alcohol **10** was converted to the isomeric carbamate **14** by reaction with the appropriate isocyanate. The oxygen and sulphur linked compounds **21**, **24**, **25** and **26** were prepared as shown in Scheme 3. The diamine **5** was converted to the thiol **16** with carbon disulphide and then methylated to give **17**. Oxidation of **17** with potassium permanganate gave the sulphone **18** which was displaced with benzyl 2-hydroxyacetate to give **19**. Debenzylation of **19** followed by amide coupling gave the ether linked compounds **21a-b**. For the sulphur linked compounds **24**, **25** and **26**, thiol **16** was alkylated with *tert*-butyl-2-bromoacetate to give **22** which was deprotected with trifluoroacetic acid to give the acid **23**. Amide coupling gave the thioether **24** and oxidation of **24** with potassium permanganate gave the sulphone **25.** Oxidation of **24** with 3-chloroperbenzoic acid gave the sulphoxide diastereomers **26a** and **26b** (this reaction gives a pair of diastereomers because R^2 is chiral with defined absolute stereochemistry).

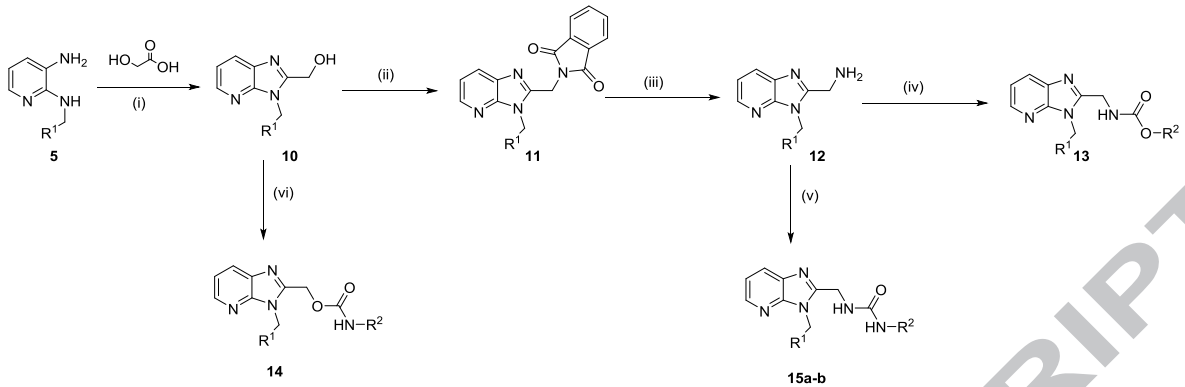

Scheme 2. Synthesis of imidazo[4,5-b]pyridine derivatives, linker modifications. Reagents and conditions: (i) glycolic acid, 150°C, 78%; (ii) phthalimide, PPh_3, DIAD, 60%; (iii) NH_2NH_2, EtOH, 97%; (iv) R^2OH, DMF, CDI, 21%; (v) R^2NCO, THF or DCM 63-68%; (vi) R^2NCO, THF, 4%.

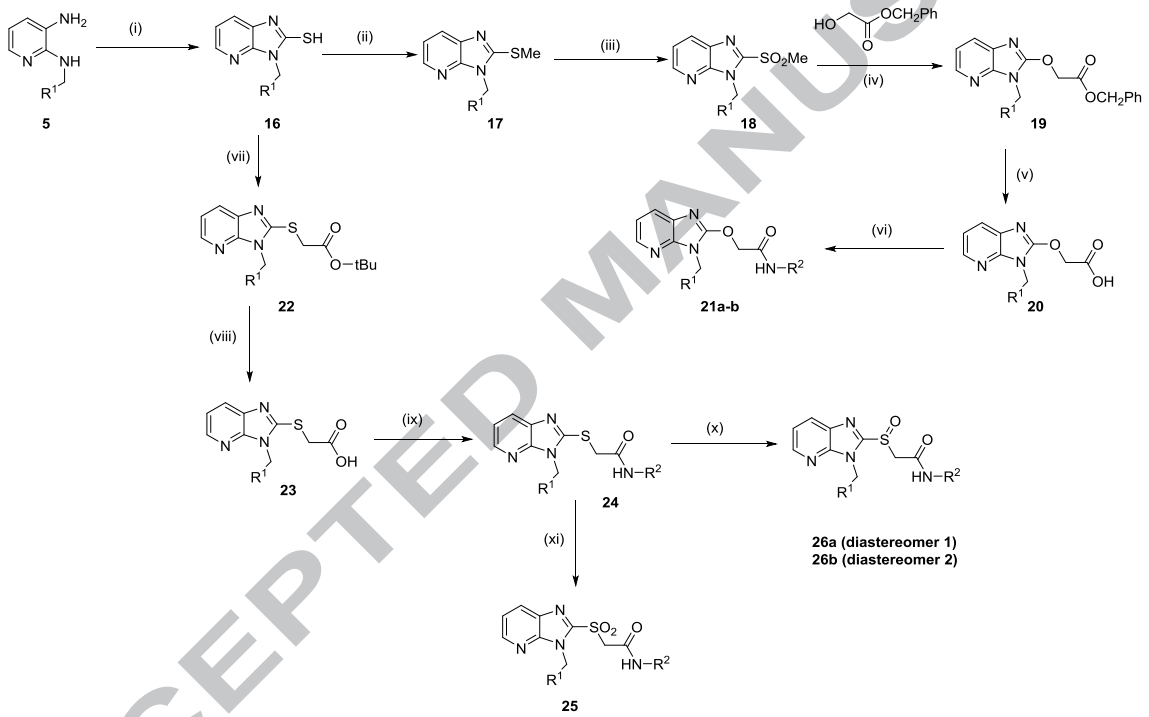

Scheme 3. Synthesis of imidazo[4,5-b]pyridine derivatives, linker modifications. Reagents and conditions: (i) CS_2, EtOH, 63-65%; (ii) MeI, EtOH, 79-85%; (iii) $KMnO_4$, AcOH, 24-35%; (iv) NaH, THF, 69-93%; (v) H_2, Pd/C, EtOAc, 1atm, 76-100%; (vi) HBTU, DMF, Et_3N, R^2NH_2, 33-40%; (vii) *tert*-butyl-2-bromoacetate, acetone, K_2CO_3, 80%; (viii) TFA, DCM, 94%; (ix) HBTU, DMF, Et_3N, R^2NH_2, 48%; (x) 3-chloroperbenzoic acid, DCM, 42% combined yield for both diastereomers; (xi) $KMnO_4$, AcOH, 22%

Compounds bearing the isomeric imidazo[4,5-c]pyridine core were synthesized as shown in Scheme 4. Displacement of the bromide **27** with the appropriate benzylamine[15] gave **28** which was reduced to the diamine **29** with hydrogen and 10% Pd/C. The N-oxide **29** was reduced to the diamine **30** with iron in acetic acid followed by reaction with succinic anhydride to give the acid **31**. Amide coupling of **31** using HBTU gave the target compounds **32a-c**.

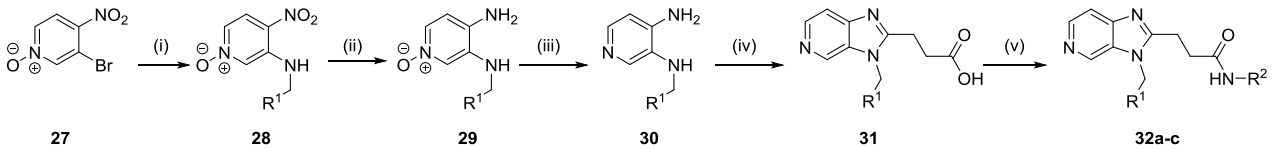

Scheme 4. Synthesis of imidazo[4,5-c]pyridine derivatives. Reagents and conditions: (i) $R^1CH_2NH_2$, *n*-propanol, 90°C, 58%; (ii) H_2, 10% Pd/C, MeOH, 1atm, 98%; (iii) Fe powder, AcOH, 90°C, 100%; (iv) succinic anhydride, dioxane, AcOH, 80°C, 31-44%; (v); HBTU, DCM, DIPEA, R^2NH_2, 16-20%

Table 2. SAR of benzyl group R^1 and amide group R^2

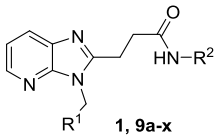

No	R^1	R^2	[a]cLogP	[b]EC IC_{50} (μM)	[c]Plasma CRA IC_{50} (μM)	[d]CL_{int} (mL/min/g liver) mouse/human
1	Ph	4-Methoxybenzyl	3.1	0.473	8.87	
9a	Ph	Benzyl	3.2	1.242		
9b	Ph	4-Fluorobenzyl	3.3	0.324		23.9/41.2
9c	Ph	4-Methylbenzyl	3.7	0.627		
9d	Ph	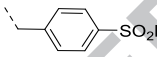	2.3	6.774		
9e	Ph	4-Chlorobenzyl	3.8	0.029	5.8	15.3/-
9f	Ph	3-Fluorobenzyl	3.3	1.252		
9g	Ph	2-Fluorobenzyl	3.3	1.251		
9h	Ph	3-Methoxybenzyl	3.1	2.974		
9i	Ph	Phenethyl	3.6	3.436		
9j	Ph	Cyclohexylmethyl	3.8	0.444	9.7	30.8/17.4
9k	Ph	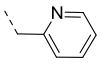	2.4	10.98		
9l	Ph	n-Butyl	3.0	8.811		
9m	Ph		3.0	0.856		
9n	Ph		3.0	2.43		
9o	Ph	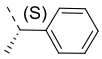	3.7	0.068	0.288	21.4/62.0
9p	Ph	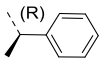	3.7	2.631		
9q	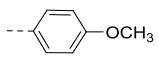	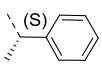	3.6	0.017	0.318	35.0/21.4
9r	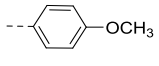	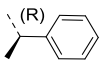	3.6	1.060	8.5	
9s	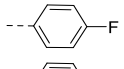	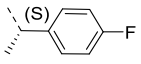	3.8	0.006	0.444	
9t	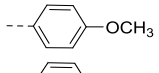	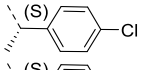	4.1	0.003	0.215	
9u	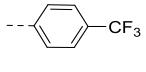	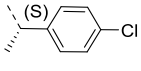	4.9	0.002	0.016	26.5/-

9v	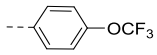	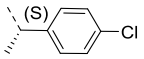	4.7	0.001	0.014	44.1/9.4
9w	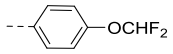	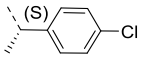	4.5	0.002	0.044	52.8/-
9x	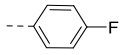	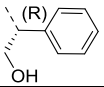	2.8	0.005	0.026	4.4/-

[a]cLogP is the octanol/water partition coefficient calculated using Stardrop™; [b]EC IC_{50} - this assay utilises LPC C16:0 as substrate and measures the release of choline; [c]CRA, (Plasma choline release assay). The physiological substrate of ATX in human plasma, LPC, is hydrolyzed by ATX to give LPA and choline. The release of choline can be detected in a two-step enzymatic reaction; [d]CL_{int} intrinsic clearance in mouse and human liver microsomes (<1 mL/min/g liver = Low; 1-5 mL/min/g liver = Medium, >5 mL/min/g liver = High)

Table 3. Linker Modifications

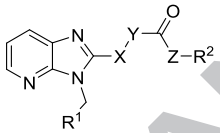

No	X	Y	Z	R^1	R^2	[a]cLogP	[b]EC IC_{50} (μM)	[c]Plasma CRA IC_{50} (μM)	[d]CL_{int} (mL/min/g liver)
13	CH_2	NH	O	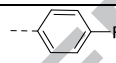	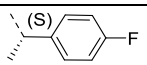	4.0	0.957		
14	CH_2	O	NH		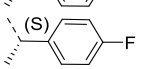	4.0	0.366	3.294	21.8
15a	CH_2	NH	NH	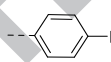	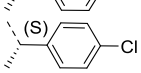	4.1	0.010	0.414	
15b	CH_2	NH	NH	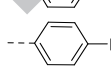	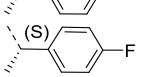	3.6	0.080	1.050	10.0
21a	O	CH_2	NH	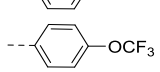	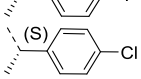	4.4	0.005	0.099	10.8
21b	O	CH_2	NH	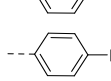	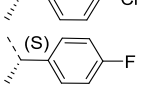	3.5	0.039	0.821	15.6
24	S	CH_2	NH	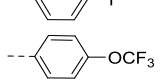	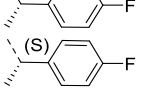	4.6	0.002	0.019	71.5
25	SO_2	CH_2	NH	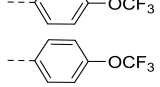	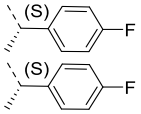	2.9	2.884		
26a	[e]SO	CH_2	NH	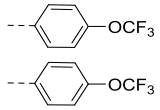	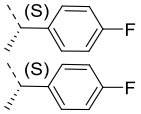	3.3	0.010	0.178	28.6
26b	[e]SO	CH_2	NH	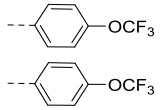	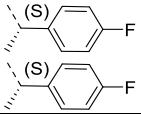	3.3	0.178	0.207	19.8

[a]cLogP is the octanol/water partition coefficient calculated using Stardrop™; [b]EC IC_{50} - this assay utilises LPC C16:0 as substrate and measures the release of choline; [c]Plasma CRA, (Plasma choline release assay). The physiological substrate of ATX in human plasma, LPC, is hydrolyzed by ATX to give LPA and choline. The release of choline can be detected in a two-step enzymatic reaction; [d]CL_{int} intrinsic clearance in mouse liver microsomes (<1 mL/min/g liver = Low; 1-5 mL/min/g liver = Medium, >5 mL/min/g liver = High). [e] Single sulphoxide enantiomer of unknown absolute stereochemistry

Table 4. Core Modification

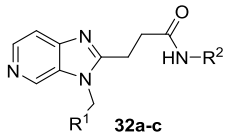

32a-c

No	R^1	R^2	[a]cLogP	[b]EC IC_{50} (μM)	[c]Plasma CRA IC_{50} (μM)	[d]CL_{int} (mL/min/g liver)
32a	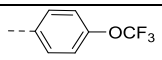	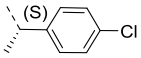	4.7	0.003	0.034	18.1
32b	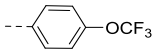	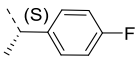	4.3	0.008	0.032	
32c	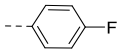	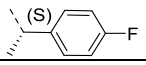	3.8	0.052	0.333	

[a]cLogP is the octanol/water partition coefficient calculated using Stardrop™; [b]EC IC_{50} - this assay utilises LPC C16:0 as substrate and measures the release of choline; [c]CRA, (Plasma choline release assay). The physiological substrate of ATX in human plasma, LPC, is hydrolyzed by ATX to give LPA and choline. The release of choline can be detected in a two-step enzymatic reaction; [d]CL_{int} intrinsic clearance in mouse liver microsomes (<1 mL/min/g liver = Low; 1-5 mL/min/g liver = Medium, >5 mL/min/g liver = High)

Table 2 summarises the effect of modifications to R^1 and R^2 in compound **9**. Looking at the R^2 group compound **9a** shows that removal of the 4-OMe substituent reduced biochemical potency whereas replacement with 4-fluoro **9b** or 4-methyl **9c** maintained activity. Introduction of the polar sulphone substituent **9d** significantly reduced potency suggesting that the 4-substituent in R^2 is accessing a lipophilic pocket in the binding site. This is further supported by the 40 fold increase in potency observed when a chloro group was introduced at the 4-position (**9a vs 9e**). Despite the improved biochemical potency for **9e** the activity seen in the plasma CRA assay was only modest. Substitution at the 2- and 3-positions of R^2 (**9f-h**) or chain extension to the phenyethyl group **9i** generally reduced potency. Saturation of the aromatic ring to give **9j** was tolerated but replacement with polar aromatic rings such as the pyridine **9k** markedly reduced potency. A major breakthrough in potency was achieved by introduction of a chiral methyl group on the benzylic carbon of R^2 which restricted the conformation of the aromatic ring (**9o and 9p**). The (*S*)-isomer **9o** was found to be 38 fold more potent than the (*R*)-isomer **9p** and the introduction of the (*S*)-methyl group resulted in an 18 fold increase in potency compared to the unsubstituted benzyl derivative (**9o vs 9a**). The separation in potency between the (*S*) and (*R*) isomers is further highlighted in compounds **9q** and **9r**. The (*S*)-isomers **9o** and **9q** also now showed improved activity in the plasma CRA assay. Combining the two potency enhancing features from **9e** and **9q** into a single molecule gave **9t** which demonstrated single digit nanomolar potency in the biochemical assay. Further optimisation of the 4-position of R^1 resulted compounds such as **9u** and **9v** which showed high potency in both the biochemical and plasma CRA assays. Due to the lipophilic nature of the ATX binding pocket the cLogP of the molecules also tended to increase as potency was optimised. We were able to address this drawback to some extent by introduction of the polar hydroxymethyl group shown in **9x**. The intrinsic clearance in mouse microsomes for **9b**, **9e**, **9j**, **9o**, **9q** and **9u-w** was found to be high and the only compound with moderate intrinsic clearance was the hydroxymethyl derivative **9x** which has the lowest cLogD of the compounds tested.

We then explored the linker portion of the molecule as shown in Table 3. The ether linked compound **21a** showed good potency but had high microsomal intrinsic clearance. The urea linked compounds **15a-b** showed a drop in potency particularly in the plasma CRA assay and the carbamates **13** and **14** and sulphone **25** were also significantly less active. The thioether analogue **24** was highly potent and, of the two corresponding sulphoxide diastereomers **26a** and **26b,** compound **26a** was more potent in the biochemical assay. The difference in potency observed between the thioether **24**, the sulphone **25**, and the sulphoxides **26a** and **26b** suggests that one of the oxygen atoms on the sulphur has an unfavourable interaction with the protein. Good potency was also achieved when the core scaffold was modified to the imidazo[4,5-*c*]pyridine ring system (Table 4). Comparative *in vitro* potency data for the published ATX inhibitor PF-8380[16] is provided in the Supplementary Information.

Having established the structural requirements for potency in both the biochemical and biomarker (CRA) assays, we evaluated key compounds in the metabolic stability assay. Disappointingly, we found that all compounds had high intrinsic clearances in mouse microsomes. To ascertain whether the *in vitro* clearance correlated to *in vivo* blood clearance, we evaluated a number of compounds in intravenous PK studies in CD-1 mice. Table 5 shows that the majority of compounds had high blood clearances when tested *in vivo* in CD-1 mice. Compound **9v**, however, had a moderate blood clearance (41 mL/min/kg). Scaling of the *in vitro* intrinsic clearance of **9v,** using the well-stirred model and incorporating free fraction, predicted an *in vivo* hepatic clearance of 25 mL/min/kg indicating that the moderate *in vivo* clearance of **9v** was driven by the high protein binding in the mouse (Table 6). The same correlation was observed in the rat. Oral bioavailability of **9v** was moderate at 41% in Balb-c *nu/nu* mice, and the compound showed a proportional increase in exposure when orally dosed at 10, 30 and 100 mg/kg (Table 7). We conducted PK studies in SD rats and found that **9v** had a reasonable PK profile in this species (Cl = 19 ml/min/kg, half life = 5.4 h, F = 28%). The compound was well tolerated in Balb-c *nu/nu* mice following five days of dosing at 100 mg/kg bid. We demonstrated that **9v** reduced LPA levels *in vivo* in MDA-MB-231-*luc* tumour bearing Balb-c *nu/nu* mice with an IC_{50} of 0.013 μM for LPA C18:1 (Supplementary Information, Section 10). The compound was effective in reducing LPA C18:1 levels *in vitro* in human plasma with an IC_{50} of 0.038 μM (LPA levels were measured using a UPLC/MS/MS assay, see Supplementary Information, Section 5). Compound **9v** was also shown to inhibit the migration of 4T1 cells with an EC_{50} of 0.025 μM in a LPC/ATX mediated transwell migration assay with recovery of inhibition in the presence of LPA (Supplementary Information, Section 6).

Table 5. Mouse Pharmacokinetic Data

No	Dose (mg/kg)	Route	[a]$t_{1/2}$ (h)	[b]CL_b (mL/min/kg	[c]Vdss (L/kg)
9q	0.5	iv	0.17	75	0.19
9u	1	iv	0.33	72	0.88
9v	1	iv	1.0	41	1.3
9w	1	iv	0.37	62	0.4
9x	1	iv	0.16	73	0.2
21a	0.5	iv	0.2	78	0.4
15b	1	iv	0.15	67	0.3
24	1	iv	0.2	81	0.3
26a	1	iv	0.22	82	0.2
32a	1	iv	0.14	73	0.2

[a]blood half life; [b]blood clearance; [c]volume of distribution

Table 6. *in vitro in vivo* correlation unadjusted and adjusted for plasma protein binding

No	Species	[a]CL_{int} (mL/min/g liver)	[b]F_u	[c]CL_{hep} pred (mLmin/kg) Unadjusted for Fu	[d]CL_{hep} pred (mLmin/kg) Adjusted for Fu	[e]CL_b *in vivo* (mL/min/kg)
9v	Mouse	44	0.018	112	25	41
9v	Rat	15	0.020	78	10	19

[a]microsomal intrinsic clearance; [b]fraction unbound, [c]predicted blood clearance scaled from *in vitro* clearance using the well-stirred liver model and unadjusted for F_u; [d]predicted blood clearance scaled from *in vitro* clearance using the well-stirred liver model and adjusted for F_u. [e]measured blood clearance

Table 7. Mouse dose escalation data

No	Dose (mg/kg)	Route	[a]Cmax (µM)	[b]AUC (µM.h))	[c]$t_{1/2}$ (h)	[d]%F
9v	10	po	3.8	3.2	1.4	41
9v	30	po	10.9	15.2	0.9	64
9v	100	po	18.1	59.3	1.3	75

[a]maximum concentration; [b]area under the curve, [c]blood half life; [d]oral bioavailability

The crystal structure of mouse ATX alone and in complex with LPAs with different acyl-chain lengths and saturations has recently been reported.[17] We solved the x-ray crystal structure of **9v** bound to mouse ATX (PDB accession code 5LIA) and this revealed that the compound interacts with the protein in an unexpected binding mode (Figure 2). The compound binds to the lipophilic acyl chain pocket of ATX and also to the LPA exit channel.[18] The inhibitor binds approximately 5Å from the catalytic centre in contrast to some ATX inhibitors reported in the literature which bind to the catalytic zinc ions and/or threonine 209 residue.[19 20] This mode of binding which avoids interaction with the catalytic zinc ions may offer selectivity advantages over other inhibitors.

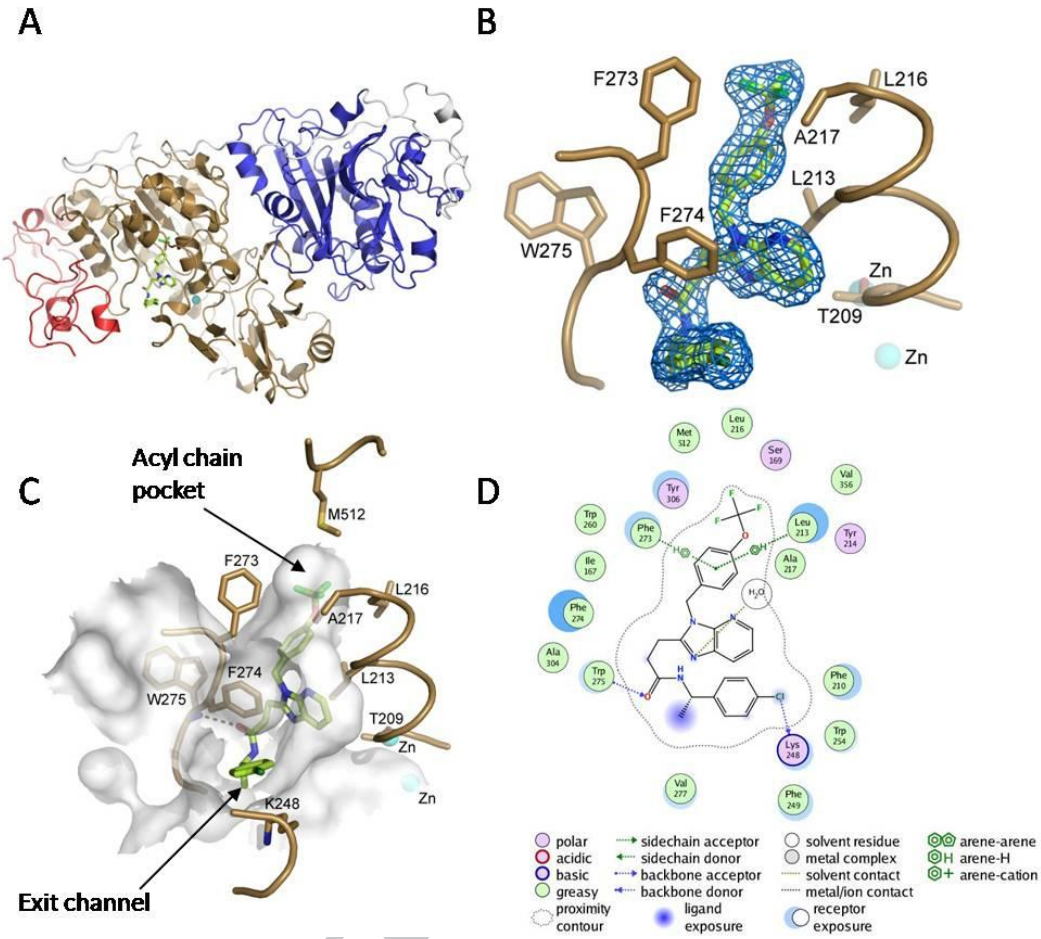

Figure 2. Crystal structure of murine ATX (mATX) in complex with 9v determined at 1.92 Å resolution (PDB 5LIA): (A) Cartoon representation of the domain organisation of mATX highlighting the compound-binding site. The somatomedin B-like domains 1 and 2 (SMB), catalytic and nuclease-like domains (NLD) are coloured red, brown and blue, respectively. The active site Zn^{2+} ions are shown as cyan spheres. **9v**, which binds to the catalytic domain, is shown as a stick representation (C: limon; N: blue; O: red; F: green; Cl: dark green); (B) Zoomed-in view of (A) showing the $2|F_{obs}|-|F_{calc}|$ electron density map (blue mesh) for **9v** contoured at 1 σ. Key residues implicated in compound binding and the catalytic threonine (T209) are labelled. **9v** binds ~5 Å away from the active site in the LPA-substrate hydrophobic pocket and LPC exit channel; (C) Equivalent view to (B) showing the surface of the compound-binding cavity in grey. The hydrogen bond between the main chain amide of W275 and the compound carboxyamide moiety is shown as a dotted line; (D) Ligand interaction diagram for **9v** produced using Molecular Operating Environment (MOE), 2013.08; Chemical Computing Group Inc., Montreal, Canada. Panels (A)-(C) were generated using PyMOL (http://www.pymol.org).

In summary we have identified and optimised a novel series of ATX inhibitors based on the imidazopyridine scaffold.[21] This work led to the discovery of a leading compound **9v** with excellent enzyme potency and drug-like properties. The compound potently inhibited the production of LPA in human plasma and has suitable PK properties for *in vivo* efficacy studies. We are currently evaluating the lead compound **9v** (CRT0273750) in ATX/LPA-dependent models of cancer.

Supplementary Data

Supplementary information associated with this article can be found in the online version.

Compound **9v** (CRT0273750) can be sourced from the XimBio reagent portal (http://www.ximbio.com).

References

1. Liu, S.; Umezu-Goto, M.; Murph, M.; Lu, Y.; Liu, W.; Zhang, F.; Yu, S.; Stephens, L. C.; Cui, X.; Murrow, G.; Coombes, K.; Muller, W.; Hung, M. C.; Perou, C. M.; Lee, A. V.; Fang, X.; Mills, G. B., *Cancer Cell* **2009,** *15*, 539.
2. Houben, A. J.; Moolenaar, W. H., *Cancer Metastasis Rev* **2011,** *30*, 557.
3. Leblanc, R.; Peyruchaud, O., *Exp Cell Res* **2015,** *333*, 183.
4. van Meeteren, L. A.; Moolenaar, W. H., *Prog Lipid Res* **2007,** *46*, 145.
5. Moolenaar, W. H.; Houben, A. J.; Lee, S. J.; van Meeteren, L. A., *Biochimica et biophysica acta* **2013,** *1831*, 13.
6. Knowlden, S.; Georas, S. N., *J Immunol* **2014,** *192*, 851.
7. Choi, J. W.; Herr, D. R.; Noguchi, K.; Yung, Y. C.; Lee, C. W.; Mutoh, T.; Lin, M. E.; Teo, S. T.; Park, K. E.; Mosley, A. N.; Chun, J., *Annu Rev Pharmacol Toxicol* **2010,** *50*, 157.
8. Zhao, Y.; Natarajan, V., *Biochimica et biophysica acta* **2013,** *1831*, 86.
9. Tager, A. M.; LaCamera, P.; Shea, B. S.; Campanella, G. S.; Selman, M.; Zhao, Z.; Polosukhin, V.; Wain, J.; Karimi-Shah, B. A.; Kim, N. D.; Hart, W. K.; Pardo, A.; Blackwell, T. S.; Xu, Y.; Chun, J.; Luster, A. D., *Nature medicine* **2008,** *14*, 45.
10. Willier, S.; Butt, E.; Grunewald, T. G., *Biology of the cell / under the auspices of the European Cell Biology Organization* **2013,** *105*, 317.
11. Castagna, D.; Budd, D. C.; Macdonald, S. J.; Jamieson, C.; Watson, A. J., *J Med Chem* **2016,** *59*, 5604.
12. Discovery of GLPG1690: A first-in-class autotaxininhibitor in clinical development for the treatment of IPF, 251st American Chemical Society National Meeting. 2016.
13. Ferguson, C. G.; Bigman, C. S.; Richardson, R. D.; van Meeteren, L. A.; Moolenaar, W. H.; Prestwich, G. D., *Organic letters* **2006,** *8*, 2023.
14. Albers, H. M.; van Meeteren, L. A.; Egan, D. A.; van Tilburg, E. W.; Moolenaar, W. H.; Ovaa, H., *J Med Chem* **2010,** *53*, 4958.
15. Nishiwaki, N.; Nishida, Y.; Tominaga, E.; Ariga, M., *Tetrahedron Letters* **2007,** *48*, 4361.
16. Gierse, J.; Thorarensen, A.; Beltey, K.; Bradshaw-Pierce, E.; Cortes-Burgos, L.; Hall, T.; Johnston, A.; Murphy, M.; Nemirovskiy, O.; Ogawa, S.; Pegg, L.; Pelc, M.; Prinsen, M.; Schnute, M.; Wendling, J.; Wene, S.; Weinberg, R.; Wittwer, A.; Zweifel, B.; Masferrer, J., *J Pharmacol Exp Ther* **2010,** *334*, 310.
17. Nishimasu, H.; Okudaira, S.; Hama, K.; Mihara, E.; Dohmae, N.; Inoue, A.; Ishitani, R.; Takagi, J.; Aoki, J.; Nureki, O., *Nat Struct Mol Biol* **2011,** *18*, 205.
18. Moolenaar, W. H.; Perrakis, A., *Nat Rev Mol Cell Biol* **2011,** *12*, 674.
19. Hausmann, J.; Kamtekar, S.; Christodoulou, E.; Day, J. E.; Wu, T.; Fulkerson, Z.; Albers, H. M.; van Meeteren, L. A.; Houben, A. J.; van Zeijl, L.; Jansen, S.; Andries, M.; Hall, T.; Pegg, L. E.; Benson, T. E.; Kasiem, M.; Harlos, K.; Kooi, C. W.; Smyth, S. S.; Ovaa, H.; Bollen, M.; Morris, A. J.; Moolenaar, W. H.; Perrakis, A., *Nat Struct Mol Biol* **2011,** *18*, 198.
20. Stein, A. J.; Bain, G.; Prodanovich, P.; Santini, A. M.; Darlington, J.; Stelzer, N. M.; Sidhu, R. S.; Schaub, J.; Goulet, L.; Lonergan, D.; Calderon, I.; Evans, J. F.; Hutchinson, J. H., *Mol Pharmacol* **2015,** *88*, 982.
21. Stockley, M. L.; MacDonald, E. C.; Shah, P.; Jordan, A.; Hitchin, J.; Hamilton, N. PCT Int. Appl. WO2016124939. 2016.

Graphical abstract

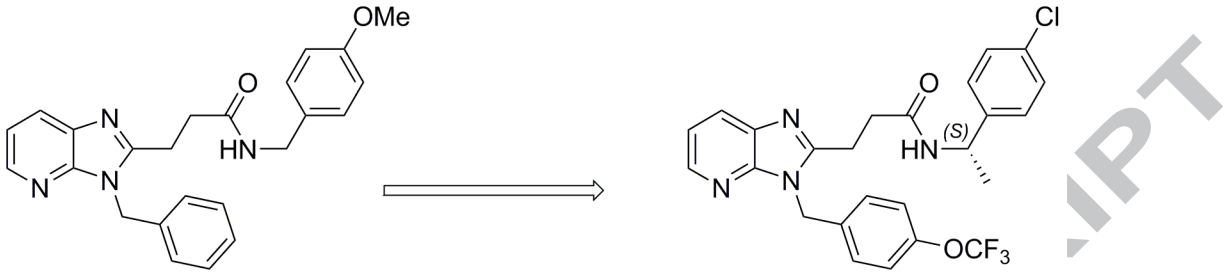

HTS Hit

ATX IC_{50} = 0.473μM

Compound 9v (CRT0273750)

ATX IC_{50} = 0.001μM